# Uniting Gradual and Abrupt SET Processes in Resistive Switching Oxides

Karsten Fleck,[1,*] Camilla La Torre,[1] Nabeel Aslam,[2] Susanne Hoffmann-Eifert,[2] Ulrich Böttger,[1] and Stephan Menzel[2]

[1]*Institute of Materials in Electrical Engineering and Information Technology II, RWTH Aachen University, 52074 Aachen, Germany*

[2]*Peter Grünberg Institute 7, Forschungszentrum Jülich GmbH, 52425 Jülich, Germany*

(Received 27 July 2016; revised manuscript received 14 October 2016; published 27 December 2016)

Identifying limiting factors is crucial for a better understanding of the dynamics of the resistive switching phenomenon in transition-metal oxides. This improved understanding is important for the design of fast-switching, energy-efficient, and long-term stable redox-based resistive random-access memory devices. Therefore, this work presents a detailed study of the SET kinetics of valence change resistive switches on a time scale from 10 ns to $10^4$ s, taking $Pt/SrTiO_3/TiN$ nanocrossbars as a model material. The analysis of the transient currents reveals that the switching process can be subdivided into a linear-degradation process that is followed by a thermal runaway. The comparison with a dynamical electrothermal model of the memory cell allows the deduction of the physical origin of the degradation. The origin is an electric-field-induced increase of the oxygen-vacancy concentration near the Schottky barrier of the $Pt/SrTiO_3$ interface that is accompanied by a steadily rising local temperature due to Joule heating. The positive feedback of the temperature increase on the oxygen-vacancy mobility, and thereby on the conductivity of the filament, leads to a self-acceleration of the SET process.

DOI: 10.1103/PhysRevApplied.6.064015

## I. INTRODUCTION

In recent years, the phenomenon of bipolar resistive switching in transition-metal oxides based on the valence change mechanism (VCM) has gained much attention for the use as an alternative nonvolatile memory technology in redox-based resistive random-access memory (ReRAM) [1–3]. Digital information in these VCM cells is encoded in different resistance states, which can be changed by appropriate electrical signals. As the conventional memory technologies like NAND flash approach their physical scaling limits, ReRAM appears to be a viable replacement due to its superior scalability, good endurance of about $10^{12}$ cycles, and fast device operation down to 100 ps [4–7]. ReRAM devices are also in the discussion for logic-in-memory applications and for pattern-recognition tasks in neuromorphic circuits [8], thus showing multiple fields for potential applications besides data storage [9].

VCM cells have a bipolar operation scheme, which means that different voltage polarities are needed for the SET, i.e., switching the cell from the high resistive state (HRS) to the low resistive state (LRS), and the RESET, i.e. switching it back to the HRS. Basically, a VCM cell consists of a metal-insulator-metal stack with a typically binary or ternary transition-metal oxide ($HfO_2$, $TiO_2$, $Ta_2O_5$, $SrTiO_3$) as the insulating layer [1,10]. The origin of this resistance change is the migration of mobile donors (here oxygen vacancies) inside of the oxide and a corresponding valence change of the cation sublattice [1]. Since its defect chemistry has been thoroughly studied, strontium titanate (STO) is often considered a model material [11]. The polarity dependence of VCM-type resistive switching is usually attributed to the Schottky barrier that forms at the metal-oxide interface [12,13]. By choosing electrodes with significantly different work functions and oxygen affinities, the active interface can be determined. Here, it is the Pt/STO interface since the work function of platinum is significantly higher compared to TiN (5.65 eV compared to 4.3 eV) [14].

Most cells require an initial electroforming process during which oxygen is locally removed from the oxide, thus leading to the formation of a conductive filament [1]. During the SET operation, the oxygen vacancies are attracted by a negative-voltage bias applied to the active electrode, thereby increasing the donor concentration at the Pt/STO Schottky interface of the filament. This increase results in a low cell resistance, the LRS. By application of a positive voltage, the oxygen vacancies are repelled from the active electrode, thus decreasing the oxygen-vacancy concentration and rebuilding the Schottky barrier. As a result, the resistance state of the cell changes into the HRS.

The kinetics of both switching processes are known to be highly nonlinear [15–21]. This nonlinearity of the switching kinetics is an essential requirement for the memory function that aims to combine fast switching with high retention. Both states, HRS and LRS, should be stable at low voltages, while the cell should switch at only moderately higher voltages. This requirement is summarized

*fleck@iwe.rwth-aachen.de

 

under the so-called voltage time dilemma [22,23]. As was already discussed in previous works, the current through the cell increases the local temperature in the filament by means of Joule heating. The higher temperature results in an increased mobility of the oxygen vacancies, thus enabling a faster switching process [16–17,19,22,24–26].

Here, we report an experimental study of the SET kinetics of resistive switching cells based on STO covering 12 orders of magnitude between 10 ns and $10^4$ s. An accurate analysis of the transient currents reveals that the SET process starts with a slow, gradual resistance change that is followed by a much faster runaway. This development is not only present in the STO devices, which are used as model devices in this work. Therefore, some key aspects of this work will also be discussed for the $Ta/TaO_x/Pt$ device discussed in Refs. [24,27]. Measurements on three additional stacks are presented in Figs. S1–S3 in the Supplemental Material [28].

Both processes, gradual resistance change and abrupt runaway, have been demonstrated in the literature, but they have usually been discussed separately due to different means of experimental analysis. Gradual processes have been studied by pulse sequences, with the device resistance measured after each pulse [29–32]. However, this method does not provide any information on the transient changes during the pulses. Conventional pulse measurements, on the other hand, often do not provide the current resolution necessary for identifying the often much less pronounced gradual effect [17,18,24,27,33,34]. In contrast to previous works that focused on either the gradual switching by pulse sequences [29–32] or the spontaneous runaway [18,17,24, 27,33,34], this work aims to describe the complete SET process as a whole. For this reason, the dynamical compact model proposed by Siemon *et al.* [35] has been adapted regarding the electrical properties to match the dynamic behavior of the Pt/STO/TiN devices. The simulation results, which describe the experimental data well, clearly propose the continuous increase of the oxygen-vacancy concentration in the gradual phase. The observation of the oxygen-vacancy drift arising already in the early stages of the SET event has strong consequences for the physical description of the SET process in VCM-type resistive switching devices, which are discussed in this paper.

## II. EXPERIMENT

The VCM-type resistive switching devices utilized in this study are built from nanocrossbar structures measuring $(100 \times 100)\,nm^2$ built on thermally oxidized silicon substrates. The layer stack from bottom to top is composed from 30 nm Pt/8 nm $SrTiO_3$/30 nm TiN [see Fig. 1(a)]. The electrode layers are deposited by sputtering. The ultrathin oxide layer is grown at 360 °C by plasma-assisted atomic-layer deposition, followed by an annealing step in nitrogen atmosphere at 600 °C to promote crystallization. Details on the atomic-layer-deposition process and integration issues are described elsewhere [36–38]. VCM cells usually require an initial electroforming step before they can be switched resistively. For the partly crystallized ultrathin STO layers, around 50% of the cells are already in the LRS, thus requiring no additional electroforming. The remaining cells are formed using a voltage ramp with a current compliance of $-10\ \mu$A, with the majority (approximately 60%) of them forming at less than $-2$ V. Figure 1(b) shows a forming curve of a Pt/STO/TiN nanocrossbar (the red curve) together with a typical *I-V* curve of the later resistive switching (the blue curves). Starting in the HRS, the current increases gradually with an increasing negative voltage until the SET at $-1$ V, marked by a rapid rise in current. Contrary to the SET, the RESET, which starts at 1.4 V, has a more gradual nature. For reasons of compatibility to the pulse measurements described in the following, the dc *I-V* curves are also measured without any current compliance.

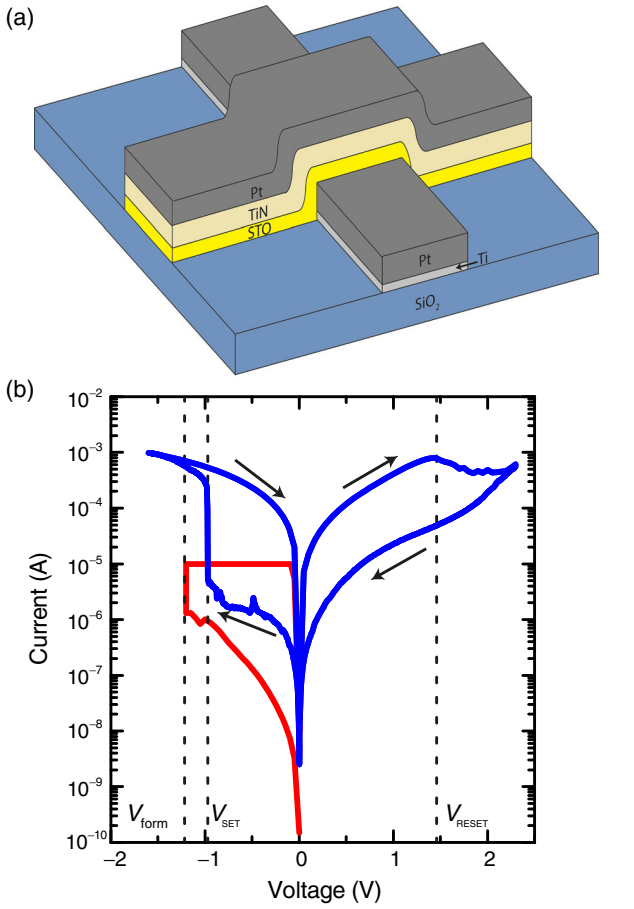


FIG. 1. (a) Geometry of the $(100 \times 100)\,nm^2$ crossbar devices composed of Pt/8 nm $SrTiO_3$/TiN. All voltages are given with respect to the bottom electrode. (b) Current-voltage characteristics of the forming (red line) and switching (blue lines) of a typical Pt/STO/TiN cell. The dashed markings indicate the forming, SET, and RESET voltages.

For the electrical measurement of the transient-current response upon voltage stress, two different setups fitting different time scales are used. On a time scale below 1 s,

pulse measurements are performed using a Keithley 4200-SCS equipped with a 4225-PMU and two remote amplifiers. The voltage pulses are applied at one channel of the PMU, which is connected to the platinum bottom electrode. Meanwhile, the other channel, which is connected to the titanium-nitride top electrode, is used for precision measurement of the transient current. Each cycle consists of a total of four single pulses. Every second cycle is used as a preparation cycle with fixed parameters. The test cycles (i.e., every other cycle) use a SET with systematically varied parameters. All cycles started with a 10 $\mu$s RESET pulse of 2.3 V, which puts the cell in the target HRS of about 100–200 k$\Omega$ verified by a −0.5 V, 1 ms READ. If the target resistance is not reached, the results of this cycle are discarded. Afterwards, a SET pulse switches the cell back to the LRS and a second READ verifies the resistance change and completes the cycle. Whereas the SET pulse of the preparation cycles is kept at a 10 $\mu$s duration and −1.4 V, the SET parameters, i.e., the pulse width and the amplitude, of the remaining test cycles are varied systematically. Starting with a 100-ns-long voltage pulse at −1.5 V, the SET amplitude is reduced in steps of 20 mV with every test cycle until no switching is observed in three consecutive test cycles. In this case, the SET pulse length is increased by a factor of 10 and the voltage is reset to −1.5 V. This method is repeated up to a pulse length of 1 s, where the PMU reaches its limitations.

Electrical measurements on the time scale above 1 s are performed using a Keithley 2636A source meter, with the time measured by the internal clock of the measurement computer. The state of the cell is defined by a bipolar-voltage sweep run between −1.5 and 2.3 V, respectively, with a slew rate of 1 V/s, first setting the cell and then resetting it to the desired HRS. Afterwards, a constant negative voltage between −0.75 and −1.2 V is applied for up to $10^5$ s to set the cell into the LRS. In a case where the SET event occurs before the end of this period, the voltage is maintained for about 20 s and then reduced to 0 V to avoid damaging the cell by constant high currents.

The temporal evolution of the voltage signals applied for both pulse schemes are depicted in Figs. 2(a) and 2(b), respectively. Figures 2(c) and 2(d) show exemplary current transients during the SET operation. The 10 $\mu$s pulse at −1.2 V, depicted in Fig. 2(c), exhibits two nearly constant current levels at about −10 $\mu$A (HRS) and −380 $\mu$A (LRS), with a rather spontaneous transition from the absolute lower level to the higher after about 6.5 $\mu$s. The time passed between the pulse amplitude reaching 90% of its maximum value and the beginning of this SET transition is named $t_{SET}$. When comparing the transient current of the −1.2 V pulse to the transient current of a −0.8 V pulse [see Fig. 2(d)], the most obvious difference is a linear increase of the HRS current from −2.74 to −16 $\mu$A before the SET event happens at 511 s. Its slope, termed pre-SET-slope, is extracted from a linear fitting of the current (the solid black line), starting at its

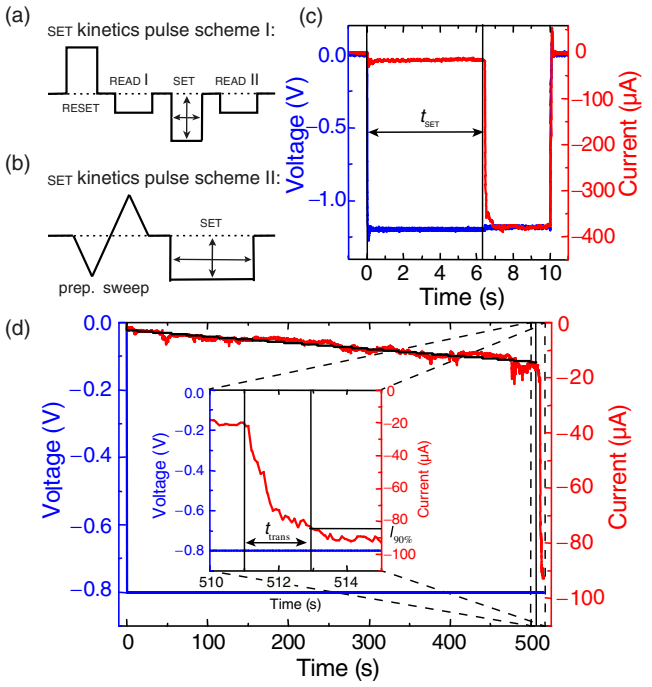


FIG. 2. Measurement schemes for the pulse measurements with SET pulse lengths (a) below 1 s and (b) above 1 s. Voltage and current transients showing two SET events on different time scales are shown in (c) and (d). (c) For a 10 $\mu$s pulse at a −1.2 V amplitude, the SET occurs after 5.8 $\mu$s. (d) A constant voltage of −0.8 V is applied to the cell. Before the SET event after 511 s, the current increases linearly. The solid black line represents the linear fit used to quantify the pre-SET-slope. (Inset) Definition of the transition time.

beginning and ending at $t_{SET}$. The origin of this linear degradation in the HRS resistance and the reason for the degradation being unnoticeable in faster pulses is the focus of Sec. IV. Another important difference between the high-voltage fast SET [see Fig. 2(c)] and the low-voltage slow SET becomes obvious only if one takes an even closer look at the SET transition itself [see the inset of Fig. 2(d)]. In fact, the SET transition exhibits a gradual nature, and, for the low-voltage SET, it takes 1.9 s until the LRS is reached. This time difference between $t_{SET}$ and 90% of the absolute maximum of the current is now defined as transition time $t_{trans}$.

This transient behavior of a gradual resistance change followed by a much faster runaway has also been reported for the electroforming of $TiO_x$ and $TaO_x$ ReRAM cells [39–41]. Based on a thermal runaway, the gradual process observed in these papers is of an electronic nature and therefore is volatile.

With the aim of testing whether the degradation of the HRS resistance before the SET is volatile (or nonvolatile), the measurements in Figs. 2(c) and 2(d) are repeated with pauses of 1 s duration every 10 s during which no voltage is applied to the cell. An example of such a SET with pauses is presented in Fig. 3(a). No difference in the degradation is found and the current level after the pause is the same as

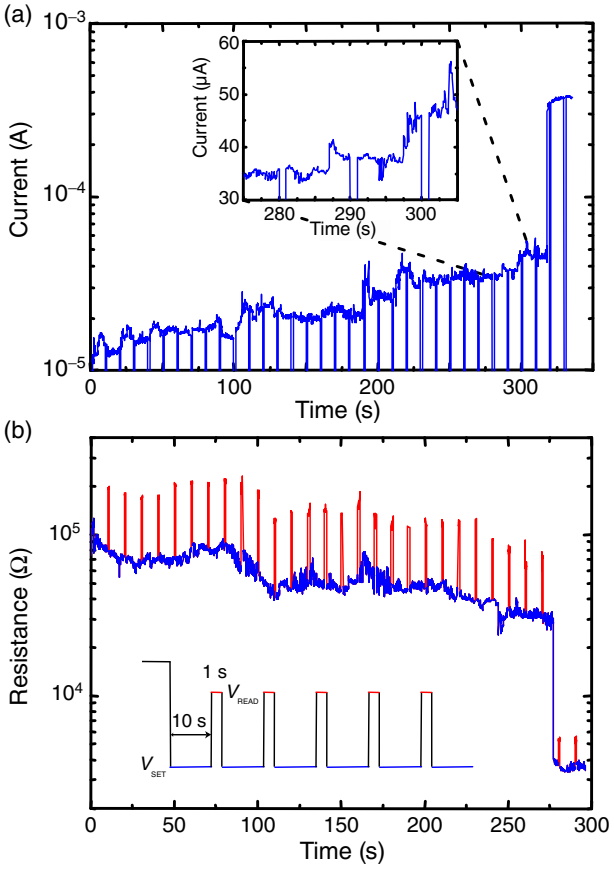


FIG. 3. (a) Transient current during a paused measurement at −0.85 V, with pauses at 0 V of 1 s duration every 10 s. The enlargement in the inset demonstrates that the cell resistance does not relax during the pauses. (b) Resistance degradation due to an applied voltage of −0.88 V (blue line) with intermediate READ pulses (red lines) at −0.5 V.

before it. Consequently, the resistance degradation is at least stable on a time scale of 1 s, and purely electronic effects can be excluded as its origin.

As a variation of this experiment, the voltage is reduced not to 0 V but instead to a READ voltage of −0.5 V. A schematic of the applied pulse sequence is depicted in the inset of Fig. 3(b). An exemplary resistance vs time plot of a −0.88 V pulse [see Fig. 3(b)] reveals that the resistance measured during the READ pulses follows the resistance degradation.

Note that experimental findings of a linearly increasing current prior to the SET transition are not only made on STO-based resistive switches. Instead, analog experiments reveal the same behavior also for $TaO_x$-based devices (see Fig. 4). The measurements are conducted on the same samples that were used by Nishi [42]. They consist of a $Ta/TaO_x/Pt$ stack with an 11-nm-thick thermally oxidized $TaO_x$ as functional oxide and $(25 \times 25)\,\mu m^2$ top electrodes. The applied pulse schemes are the same as those used with the STO devices, aside from a higher RESET amplitude of 2.5 V and a higher maximum SET amplitude of −2.2 V. Another example measured on a $ZrO_x$-based device is

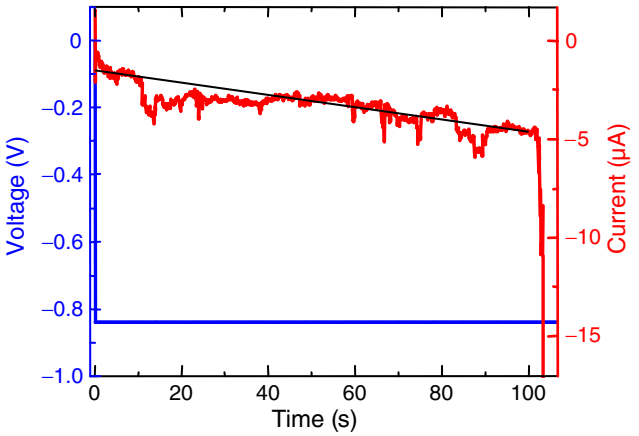


FIG. 4. (a) Current transient of a −0.84 V pulse applied to a $(25 \times 25)\,\mu m^2$ $Pt/TaO_x/Ta$ cell (the same stack as was used in Refs. [24,27]); the pre-SET-slope is very prominent.

found in Fig. S1, together with additional measurements on different STO- and $TaO_x$-based devices (see Figs. S2 and S3 in the Supplemental Material [28]).

## III. DYNAMICAL COMPACT MODEL

The used compact model is based on the memristive model for $TaO_x$ by Siemon *et al.* [35]. According to the authors of Ref. [13], the switching is thought to occur by a modulation of the barrier transport resulting from the change in ion concentration close to the appropriate interface. Thus, for the zero-dimensional compact model, the filamentary region is split into two parts called plug and disc. The plug describes the well-conducting region that consists of a reduced oxide with a high concentration of oxygen vacancies. The region between the front of the plug and the Pt electrode is called disc. Switching is characterized by a change of the oxygen-vacancy concentration in the disc. The donor concentration in the plug, $N_{\mathrm{plug}}$, remains constant during switching and serves as an oxygen-vacancy reservoir for the disc. The oxygen-vacancy concentration in the disc, $N_{\mathrm{disc}}$, is used as the state variable. The geometrical dimensions of the filament are fixed. However, in the LRS, the concentration of oxygen vacancies in the disc equals the concentration in the plug, creating a continuous and homogeneous filament.

The change of oxygen vacancies in the disc can be modeled in terms of an ionic current $I_{\mathrm{ion}}$ between plug and disc, which depends on the local temperature and the electric field. Ionic hopping conduction over a potential barrier $\Delta W_A$ modified by the electric field in the disc $E_{\mathrm{disc}}$ at temperature $T$ is described by the Mott-Gurney law [14]:

$$I_{\mathrm{ion}} = A z_{V_O} e c_{V_O} a \nu_0 \exp\left(-\frac{\Delta W_A}{k_B T}\right) \sinh\left(\frac{a z_{V_O} e E_{\mathrm{disc}}}{2 k_B T}\right), \tag{1}$$

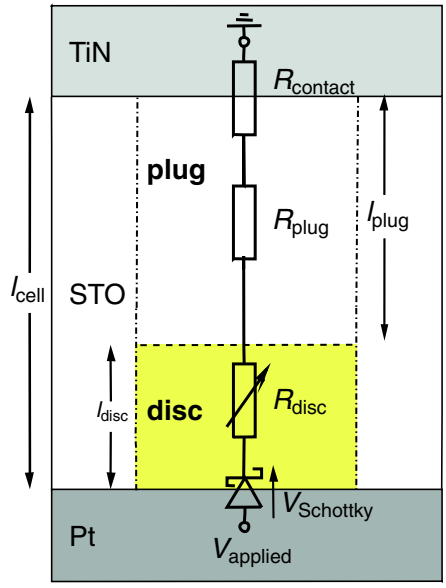


FIG. 5. Equivalent circuit diagram representing the electrical model of the TiN/STO/Pt device. As in the measurements, the voltage is applied to the bottom electrode.

where $a$ equals the hopping distance, $v_0$ the attempt frequency, and $A$ the cross-sectional area of the filament, with $A = \pi r_{\mathrm{fil}}^2$ and filament radius $r_{\mathrm{fil}}$. In addition, $z_{V_\mathrm{O}}$ is the oxygen-vacancy-charge number, $e$ the elementary charge, and $k_B$ the Boltzmann constant. The concentration $c_{V_\mathrm{O}}$ is modeled as an average of plug and disc concentration:

$$c_{V_\mathrm{O}} = \frac{N_{\mathrm{plug}} + N_{\mathrm{disc}}}{2}. \tag{2}$$

The change of the disc concentration is then

$$\frac{dN_{\mathrm{disc}}}{dt} = -\frac{1}{z_{V_\mathrm{O}} e A l_{\mathrm{disc}}} I_{\mathrm{ion}}, \tag{3}$$

where $l_{\mathrm{disc}}$ is the length of the disc. The oxygen-vacancy concentration in the disc is kept between limits of $N_{\mathrm{disc,min}}$ and $N_{\mathrm{disc,max}}$ by converting every calculated value outside of these limits to $N_{\mathrm{disc,min}}$ and $N_{\mathrm{disc,max}}$, respectively. No ion flux across the metal-oxide interfaces is considered. The temperature and the local electric field in the disc are obtained from the thermal and electrical models, respectively.

The equivalent circuit diagram of the TiN/STO/Pt device is shown in Fig. 5. The Pt/STO interface is modeled by a Schottky diode whose barrier is varied by $N_{\mathrm{disc}}$. In contrast to the original model [35], the HRS is modeled solely by the current through the filament, and no additional current path is considered. The leakage current is neglected, as the investigated device area in this work is 4 orders of magnitude smaller than in the reference work. The SET occurs with negative voltage applied to the Pt bottom electrode and, thus, in the reverse direction of the diode. Thermionic-field emission describing tunneling of thermally exited electrons across a potential barrier is assumed to be the dominating current contribution in the reverse direction of the diode [43]:

$$\begin{aligned} I_{\mathrm{Schottky},V<0\ \mathrm{V}} &= -AA^* \frac{T_S}{k_B} \sqrt{\pi E_{00} e \left( -V_{\mathrm{Schottky}} + \frac{\phi_{Bn}}{\cosh^2\left(\frac{E_{00}}{k_B T}\right)} \right)} \\ &\quad \cdot \exp\left(\frac{-e\phi_{Bn}}{E_0}\right) \left[ \exp\left(\frac{-eV_{\mathrm{Schottky}}}{\varepsilon'}\right) - 1 \right]. \end{aligned} \tag{4}$$

$A^*$ denotes the effective Richardson constant and $e\phi_{Bn}$ the effective barrier height. $V_{\mathrm{Schottky}}$ is the voltage across the diode. The parameters $E_{00}$, $E_0$, and $\varepsilon'$ are defined as follows [43]:

$$E_{00} = \frac{eh}{4\pi} \sqrt{\frac{z_{V_\mathrm{O}} N_{\mathrm{disc}}}{m^* \varepsilon}}, \tag{5}$$

$$E_0 = E_{00} \coth\left(\frac{E_{00}}{k_B T}\right), \tag{6}$$

$$\varepsilon' = \frac{E_{00}}{(E_{00}/k_B T) - \tanh(E_{00}/k_B T)}. \tag{7}$$

As first approximation, the electron mass is used instead of the effective electron mass $m^*$, $h$ is the Planck constant, and $\varepsilon$ is the dielectric permittivity of the oxide. Owing to the applied electric field, the Schottky-barrier height $e\phi_{Bn_0}$ is reduced according to [43]

$$e\phi_{Bn} = e\phi_{Bn_0} - e \sqrt[4]{\frac{e^3 z_{V_\mathrm{O}} N_{\mathrm{disc}} (\phi_{Bn_0} - \phi_n - V_{\mathrm{Schottky}})}{8\pi^2 \varepsilon_{\phi_B}^3}}, \tag{8}$$

where $e\phi_n$ is the energy difference between Fermi level and conduction band and $\varepsilon_{\phi_B}$ the permittivity related to the process of image-force barrier lowering, which can differ from the static permittivity. The STO/TiN interface is modeled as Ohmic contact in the resistance $R_{\mathrm{contact}}$ combined with the series resistances of the electrodes. Ohmic conduction is assumed in plug and disc. Thus, the plug resistance $R_{\mathrm{plug}}$ and the disc resistance $R_{\mathrm{disc}}$ are calculated using

$$R_{\mathrm{plug}} = \left( \frac{l_{\mathrm{plug}}}{e z_{V_\mathrm{O}} N_{\mathrm{plug}} \mu_n A} \right) \cdot \exp\left(\frac{\Delta W_{\mathrm{ac}}}{k_B T}\right), \tag{9}$$

$$R_{\mathrm{disc}} = \left( \frac{l_{\mathrm{disc}}}{e z_{V_\mathrm{O}} N_{\mathrm{disc}} \mu_n A} \right) \cdot \exp\left(\frac{\Delta W_{\mathrm{ac}}}{k_B T}\right), \tag{10}$$

with electron mobility $\mu_n$ and length of the plug $l_{\mathrm{plug}} = (l_{\mathrm{cell}} - l_{\mathrm{disc}})$. $\Delta W_{\mathrm{ac}}$ is the activation energy of the electrons. With $V_{\mathrm{disc}}$ being the voltage across the disc

resistance, the local electric field used in Eq. (1) for the ion movement is

$$E_{\mathrm{disc}} = \frac{V_{\mathrm{disc}}}{l_{\mathrm{disc}}}. \tag{11}$$

The local temperature in the filament is increased due to Joule heating. As it was shown in a 2D model that the temperature along the filament is rather homogeneous [12], one single temperature for the whole filament is assumed. Taking into account that the power dissipation is highest in the disc, the thermal model reads

$$T = V_{\mathrm{disc}} I_{\mathrm{Schottky}} R_{\mathrm{th,eff}} + T_0. \tag{12}$$

Thereby, $R_{\mathrm{th,eff}}$ is the effective equivalent thermal resistance of the device and $T_0$ is the ambient temperature.

Using Newton's method,

$$0 = V_{\mathrm{applied}} - V_{\mathrm{Schottky}} - I_{\mathrm{Schottky}}(V_{\mathrm{Schottky}}, N_{\mathrm{disc}}, T(V)) \times [R_{\mathrm{disc}}(N_{\mathrm{disc}}, T(V)) + R_{\mathrm{plug}}(T(V)) + R_{\mathrm{contact}}] \tag{13}$$

is solved for $V_{\mathrm{Schottky}}$ at each time step, with $V_{\mathrm{applied}}$ being the applied voltage to the bottom electrode. Then all variables are updated using the new $V_{\mathrm{Schottky}}$, as well as $T$ and $N_{\mathrm{disc}}$ from the last time step [Eqs. (4)–(11)]. After that, the temperature is calculated [Eq. (12)] and, finally, the disc concentration is updated via Eqs. (1)–(3). To solve the ordinary differential equation, an Euler method is applied.

All parameters used in the simulation can be found in Table I. They are chosen within physically reasonable limits and fitted to match the HRS currents of the experimental data (see Fig. S4 in the Supplemental Material [28]) and the cell dynamics.

For the SET operation, incorporating ion diffusion would lead to an additional ionic flux from the plug to the disc, and thus in parallel to the flux driven by the electric field. Consequently, the SET transition would occur faster. However, for a sufficiently stable HRS on the considered time scale, the ion flux driven by the electric field is highly dominating and diffusion is neglected, as small adjustments in the simulation parameters for compensation are made.

TABLE I. Simulation model parameters.

| Symbol | Value | Symbol | Value |
|---|---|---|---|
| $l_{\mathrm{cell}}$ | 8 nm | $A^*$ | $6.01 \times 10^5$ A/(m$^2$K$^2$) |
| $l_{\mathrm{disc}}$ | 3 nm | $\varepsilon$ | $17\,\varepsilon_0$ |
| $r_{\mathrm{fil}}$ | 10 nm | $\varepsilon_{\phi_B}$ | $5.5\,\varepsilon_0$ |
| $z_{\mathrm{Vo}}$ | 2 | $e\phi_{Bn_0}$ | 0.3 eV |
| $a$ | 0.6 nm | $e\phi_n$ | 0.1 eV |
| $\nu_0$ | $8.3 \times 10^{12}$ Hz | $\mu_n$ | $1.75 \times 10^{-4}$ m$^2$/(Vs) |
| $\Delta W_A$ | 1.3 eV | $\Delta W_{\mathrm{ac}}$ | 0.03 eV |
| $N_{\mathrm{disc,min}}$ | $8 \times 10^{24}$ m$^{-3}$ | $R_{\mathrm{contact}}$ | 2 kΩ |
| $N_{\mathrm{disc,max}}$ | $5 \times 10^{26}$ m$^{-3}$ | $R_{\mathrm{th,eff}}$ | $11.9 \times 10^6$ K/W |
| $N_{\mathrm{plug}}$ | $5 \times 10^{26}$ m$^{-3}$ | $T_0$ | 293 K |

In the HRS, the voltage drops almost completely across the Schottky diode and the disc (see Fig. S5 in the Supplemental Material [28]). As the Schottky-barrier height is small, the dominating element in the HRS for all voltages from −0.8 to −1.5 V is the disc resistance, $R_{\mathrm{disc}}$, which is assumed to be linear dependent on the voltage. Consequently, the overall $I$-$V$ relationship in this voltage range is nearly linear (see Fig. S4 in the Supplemental Material [28]). While this assumption is certainly not true for very small voltages, it fits to the measured HRS currents of the STO device in the studied voltage range reasonably well.

## IV. RESULTS AND DISCUSSION

The experimentally determined dependence of the SET time $t_{\mathrm{SET}}$ on the applied voltage is shown in Fig. 6(a), revealing the as-expected high nonlinearity of the switching kinetics. Starting just above −0.8 V, with a spreading between 1 and $10^4$ s, the SET time decreases to a few nanoseconds at −1.49 V. In Fig. 6(b), the voltage dependence of the pre-SET-slope is depicted (note the logarithmic scale of the $y$ axis). Here also, a highly nonlinear behavior is found with pre-SET-slope values ranging from $10^{-10}$ A/s for voltages around −0.8 V to around 1 A/s for voltages below −1.1 V, thus changing by more than 10 orders of magnitude. For higher pulse amplitudes, determining the pre-SET slope becomes rather difficult. As can be seen in Fig. 7, there is a strong hyperbolic correlation between the pre-SET-slope and $t_{\mathrm{SET}}$, with pre-SET-slope = 2.58 $\mu$A/$t_{\mathrm{SET}}$ (the fit is the black dashed line). This correlation corresponds to a fixed overall current change $\Delta I = 2.58$ $\mu$A during the degradation, which is in good accord with the median $\Delta I$ of 2.02 $\mu$A directly extracted from the current transients, although the spread is rather high (first quartile, 0.16 $\mu$A; third quartile, 4.69 $\mu$A). This rather fixed $\Delta I$ explains the difficulty in determining the pre-SET-slope for higher amplitudes, as the effect of the degradation becomes smaller compared to the already higher HRS currents at these voltages. In addition, the noise level of the faster-pulse setup is higher, being on the order of around 1 $\mu$A. The third parameter extracted from the current transient [see Fig. 2(d)] is the transition time $t_{\mathrm{trans}}$ of the SET event, which is defined as the period between $t_{\mathrm{SET}}$ and the time where 90% of the maximum absolute LRS current is reached. The dependency of $t_{\mathrm{trans}}$ on the applied voltage is shown in Fig. 6(c). For low pulse amplitudes, the transition takes up to 100 s and decreases rapidly down to about 50 ns at −1.2 V.

Figure 8 shows the voltage dependence of the pre-SET-slope measured on the Ta/TaO$_x$/Pt devices already mentioned in Sec. II. The trend is very similar to the one

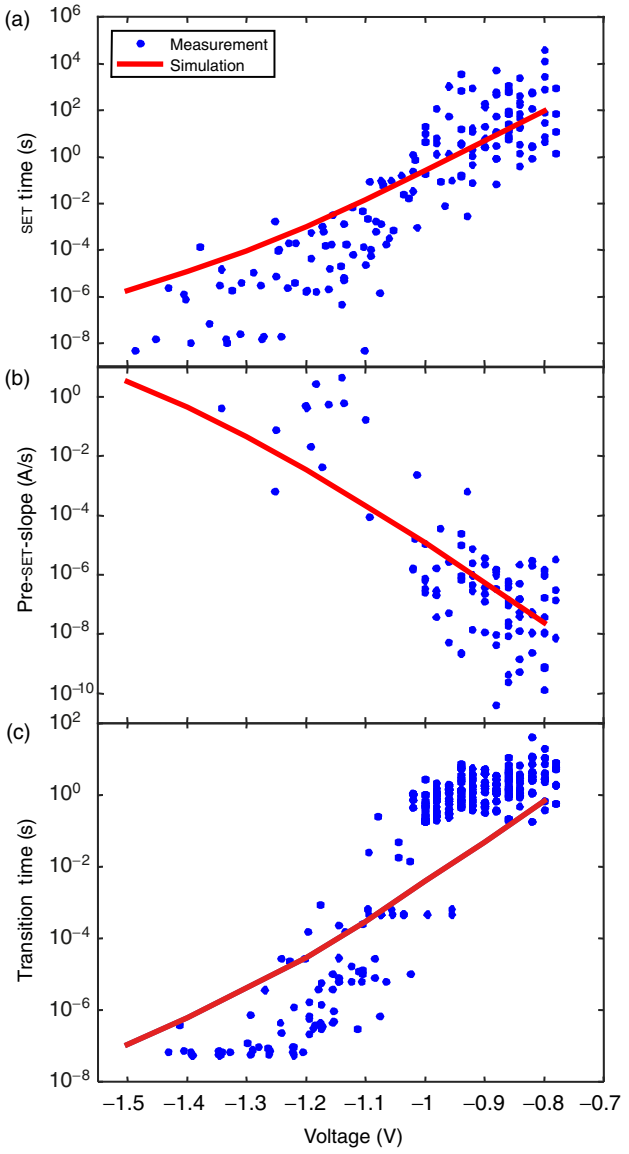


FIG. 6. (a) SET time as a function of the applied voltage. As expected, the dependency is highly nonlinear. (b) The voltage dependence of the pre-SET-slope (absolute values), which ranges over 10 orders of magnitude. (c) The transition time $t_{\mathrm{trans}}$ as a function of the applied voltage is also highly nonlinear. Experimental data is shown as blue dots and the simulation result as a red line.

observed in the STO devices (additional measurements on different samples can be found in Figs. S2 and S3 in the Supplemental Material [28]).

The measurement results on STO are compared to the simulation results obtained with the compact model [see the red lines in Figs. 6(a)–6(c)]. The overall agreement is good, validating the used model within the scope of this work. To explain the measured behavior, the simulation results are analyzed in detail below. Therefore, the current responses to eight voltage pulses, with amplitudes ranging from −0.8 to −1.5 V and a rise time of 10 ns are simulated [see

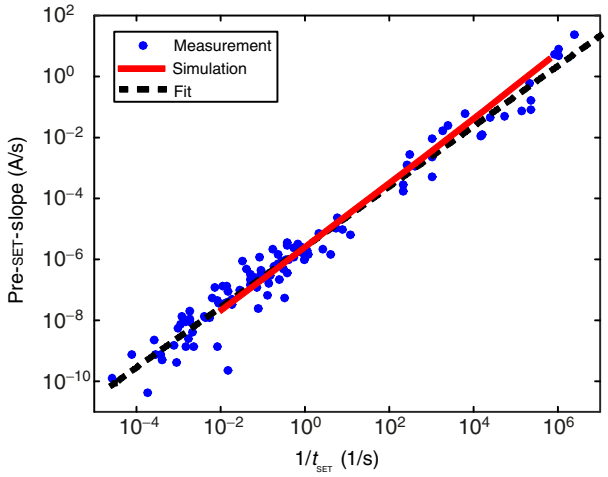


FIG. 7. The pre-SET-slope (absolute values) plotted against $1/t_{\mathrm{SET}}$ shows the direct correlation of both parameters. The solid red line represents the simulation and the dashed black line a hyperbolic fit of the measurement.

Fig. 9(a)]. At any time $t$, the present change in current is described by the derivative $\partial I(t)/\partial t$, whereas the total change in current compared to the starting level is given as $\Delta I(t)/\Delta t = [I(t) - I_{\mathrm{plateau\ start}}]/(t - t_{\mathrm{plateau\ start}})$. To compare the kind of ongoing change in current, the relation of present change to total change $[\partial I(t)/\partial t]/[\Delta I(t)/\Delta t]$ is a good indicator. It is calculated using equidistant time steps in the simulation. A ratio of 2 signifies that the current is changing twice as much in the next time step as in the whole time $\Delta t$ before. To identify the SET time and the pre-SET-slope in simulation, two criteria are defined. The point in time with a ratio of $[\partial I(t)/\partial t]/[\Delta I(t)/\Delta t] = 100$ is used for all pulses as the SET time. The resulting SET time depending on the pulse voltage is sketched together with the measurement data in Fig. 6(a), matching the overall trend of the data. To determine the pre-SET-slope of the current plateau, a linear fit at the interval between the beginning of the plateau $t_{\mathrm{plateau\ start}}$ and the point with ratio $[\partial I(t)/\partial t]/[\Delta I(t)/\Delta t] = 2$ is performed. Figure 9(b) shows the current transient for an applied voltage of −1.5 V in blue and a line with the calculated pre-SET-slope in green, respectively. The two criteria are also marked. Note that the line with the determined slope is drawn further than the interval on which it is evaluated. In good agreement with the measurement results, the fitted slopes from the simulation depend on the applied pulse voltage and increase for a higher pulse amplitude; see Fig. 6(b). To show these different slopes exemplarily in one plot, the current transients each normalized to their value at the beginning of the plateau are shown in Fig. 9(c). In this regime, a linear slope is apparent that depends on the voltage amplitude. The discontinuities are due to the numerical precision restriction, as the change in current is very small. The simulation results for the transition time $t_{\mathrm{trans}}$ are depicted in Fig. 6(c) alongside the experimental data. The parameter

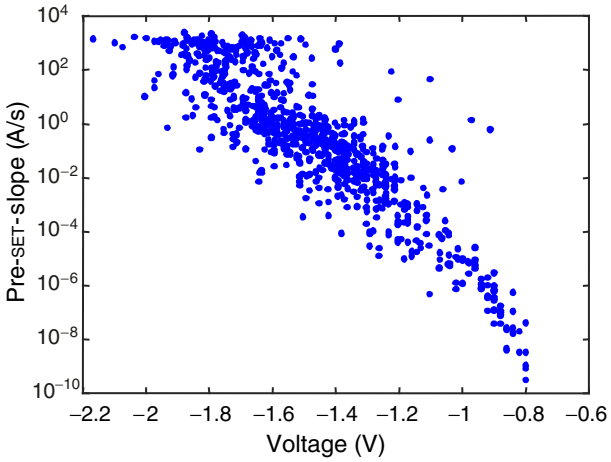


FIG. 8. The pre-SET-slope (absolute values) measured on the $TaO_x$ device has a similar voltage dependence to that measured on the STO nanocrossbars.

is obtained as the difference between the point in time with the ratio $[\partial I(t)/\partial t]/[\Delta I(t)/\Delta t] = 2$ and the one where the current reaches 90% of the absolute maximum.

To explain the linear slope in the current before the SET, current $I$, temperature $T$, and oxygen-vacancy concentration in the disc $N_{\mathrm{disc}}$ for the voltage pulses of −0.8 and −1.5 V are depicted in Figs. 10(a) and 10(b), respectively. The variation in current is induced by an increase in disc concentration and temperature, as both lower the overall resistance. The nonvolatile change in resistance before the switching event in the measured data can be explained by the change in the model's state variable $N_{\mathrm{disc}}$. On the contrary, a sole variation in temperature always leads to volatile change of the system and thus cannot be the origin of the observed slope. There is an overshoot in temperature with a varying magnitude during the abrupt current rise that is not a numerical artifact. The change in temperature is affected by both the rise in current and the concurrent drop in voltage $V_{\mathrm{disc}}$ [see Eq. (12)], causing opposing trends.

Although the current, the temperature, and the SET time differ strongly for the various pulse voltages, the overall process is quite similar. Normalizing the current to its start value and the time to the SET time gives a uniform curve shape, as illustrated in Fig. 10(c). This result underlines that the model used is a deterministic one. Statistical aspects of the SET may stem from different initial conditions in the HRS regarding, e.g., the filament shape [27,44].

The increase in vacancy concentration is field- and temperature-driven. Both field and temperature enhancement in the process of ion migration lead to a nonlinearity in switching time. But assuming exclusively field-driven migration leads to only a weak nonlinearity of very few orders of magnitude in time [15]. Consequently, the high nonlinearity in switching time of 8 orders of magnitude, with voltages between −0.8 and −1.5 V [shown in Fig. 6(a)], can be explained only with temperature enhancement. To separate the two contributions on the SET transients, the current transient for $V_{\mathrm{pulse}} = -1.5$ V is simulated with a model that equals the model described above, except that the temperature $T$ is not increased by Joule heating, so that $T = T_0$ is valid at all times [see Fig. 11(a)]. Naturally, without any temperature enhancement, the SET time increases, but the more important factor is that no abrupt switching takes place. Instead, a gradual transition over several orders of magnitude in time leads to the LRS. A gradual SET in place of an abrupt one also occurs when a SET sweep is simulated without considering Joule heating (see Fig. S6 in the Supplemental Material [28]). Consequently, an abrupt switching event is the result of a thermal runaway. This process is characterized by a positive feedback, as the current rise increases the local temperature, causing a faster change in oxygen-vacancy concentration and thereby increasing the current even further. In the case of a thermal runaway, relating the

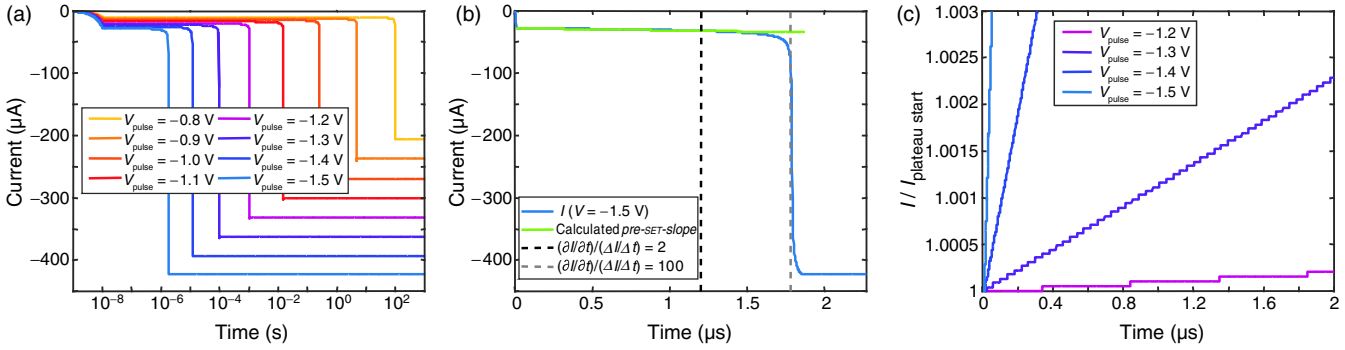


FIG. 9. (a) Simulated current transients of applied voltage pulses with amplitudes ranging from −0.8 to −1.5 V and a rise time of 10 ns. (b) Current transient with criteria marked to determine the slope of the plateau and the SET time. The slope of the current, i.e. the pre-SET-slope, is fitted linearly between the beginning of the plateau and the point for which $[\partial I(t)/\partial t]/[\Delta I(t)/\Delta t] = 2$ holds. To visualize the fitted slope, a line with the calculated slope is also plotted. The SET time $t_{\mathrm{SET}}$ is determined by the point in time with a ratio $[\partial I(t)/\partial t]/[\Delta I(t)/\Delta t] = 100$. (c) The four current transients with the highest slopes are normalized with respect to the current value at the beginning of the plateau.

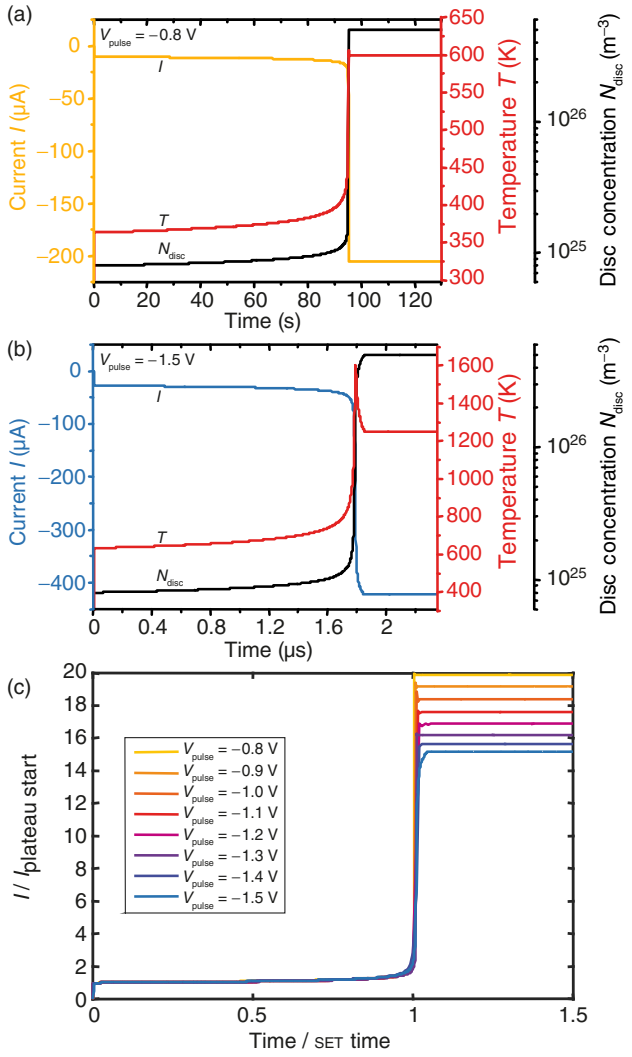


FIG. 10. Transients of current, temperature, and disc concentration of oxygen vacancies for (a) $V_{pulse} = -0.8$ V and (b) $V_{pulse} = -1.5$ V. (c) Current transients for applied voltages ranging from −0.8 to −1.5 V, with the current normalized to the start value at the beginning of the current plateau and the time normalized to the SET time of each pulse.

present change to the total change $[\partial I(t)/\partial t]/[\Delta I(t)/\Delta t]$ gives a monotonically increasing curve, as shown in Fig. 11(b). On the contrary, the gradual transition for the solely field-driven simulation is characterized by a decreasing $[\partial I(t)/\partial t]/[\Delta I(t)/\Delta t]$, as no positive but a negative feedback exists between the current rise and the driving force. The increase in current results in a decrease in disc resistance $R_{disc}$ and voltage $V_{disc}$. Thus, the electric field across the disc as a driving force for further ion movement and further resistance decrease is reduced, resulting in a negative feedback. In contrast, a short time interval slightly before and after $t = 10^3$ s shows a slightly increasing $[\partial I(t)/\partial t]/[\Delta I(t)/\Delta t]$ since a small positive feedback exists. In that interval, the electric field increases as the increase in current dominates over the decrease in disc

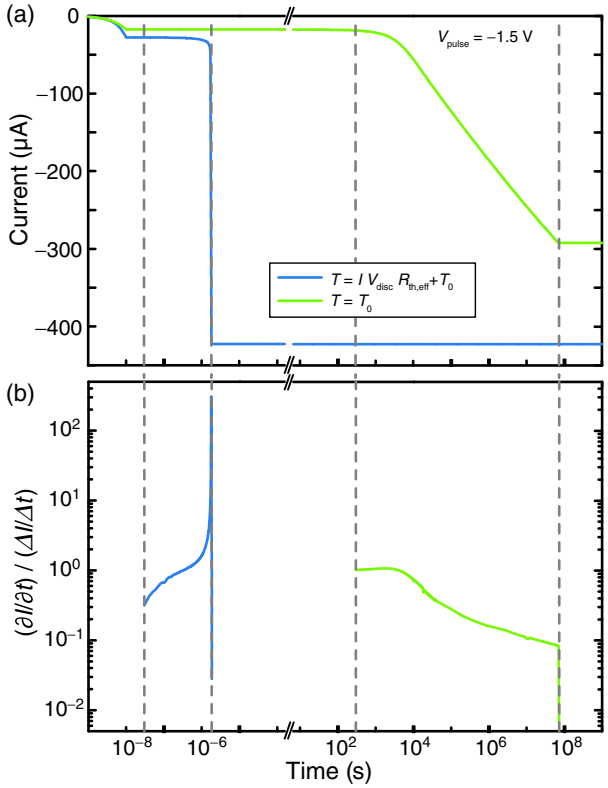


FIG. 11. Analysis of the contribution of Joule heating on the switching process, for (a) $V_{pulse} = -1.5$ V current transients and (b) $[\partial I(t)/\partial t]/[\Delta I(t)/\Delta t]$ modeled with Joule heating in blue and with the temperature held constant at $T_0$ in green. Without any thermal feedback, the SET transition is highly gradual.

resistance (see Fig. S7 in the Supplemental Material [28]). Outside the boundaries that are marked with dashed lines in Figs. 11(a) and 11(b), the derivative $[\partial I(t)/\partial t]$ is zero or is so small that calculating $[\partial I(t)/\partial t]/[\Delta I(t)/\Delta t]$ generates numerical problems.

## V. CONCLUSION

In summary, this paper presents a detailed discussion of the transient currents during the SET process in oxide-based VCM-type resistive switches, utilizing $Pt/SrTiO_3/TiN$ cells as model material. The experimental results are supported by measurements on four additional devices, among them $TaO_x$-and $ZrO_x$-based devices. This occurrence suggests that the observed phenomena are part of the general VCM switching. Phenomenologically, the SET consists of two nonvolatile processes, a gradual degradation of the HRS followed by a prominent and much faster runaway, which are actually of the same physical origin. In addition, it is shown that the duration of the runaway process called transition time is highly dependent on the applied voltage and increases for a decreasing pulse amplitude. To summarize, we describe the SET process by three parameters, the pre-SET-slope that describes the

gradual process, the SET time $t_{SET}$ marking the beginning of the runaway, and the time necessary for the transition $t_{trans}$. Through variation of the applied pulse amplitude, we demonstrate that both the pre-SET-slope and $t_{trans}$ have a highly nonlinear voltage dependence, as was shown for $t_{SET}$ in earlier works. An in-depth analysis of the pre-SET-slope reveals a hyperbolic correlation to $t_{SET}$ that points towards a defined increase of the current in HRS $\Delta I$ preceding the runaway. If higher voltages are applied, the pre-SET-slope is often unnoticed because it is easily obscured by scattering in the current signal.

By means of a physics-based dynamical compact model, we reproduce the experimentally measured transient current during a SET pulse and the voltage dependency of the above-mentioned parameters used to describe it. By analysis of the model's state variable, it is found that the pre-SET-slope originates from an increasing oxygen vacancy concentration in the disc region, thus increasing its conductivity in a nonvolatile manner. Consequently, the existence of a nonvolatile degradation process in the pre-SET regime can be seen as a clear indication that the HRS is dominated by the filament and not by any unrelated parallel current paths. The abrupt increase of the current during the runaway at $t_{SET}$ is the result of a positive feedback that is triggered by Joule heating. Checking for $[\partial I(t)/\partial t]/[\Delta I(t)/\Delta t]$ to increase monotonically is described as an option for identifying a positive feedback crucial for a runaway. Consistently, a simulation without Joule heating and only field acceleration leads to purely gradual switching.

## ACKNOWLEDGMENTS

We would like to thank Valentino Longo, Fred Roozeboom, and Erwin Kessels from the University of Technology Eindhoven for the preparation of the STO thin films. Also, we would like to thank Andreas Kindsmüller for providing the $ZrO_x$ sample, Thomas Breuer for providing the $TaO_x$ nanocrossbars, and Moritz von Witzleben, Lena Hellmich, and Alexander Idt for the measurements on the $ZrO_x$ and $TaO_x$ nanocrossbar devices presented in the Supplemental Material. This work was funded in part by the German Research Foundation (DFG) under Grant No. SFB 917.

K. F. and C. L. contributed equally to this work.

[1] R. Waser, R. Dittmann, G. Staikov, and K. Szot, Redox-based resistive switching memories—Nanoionic mechanisms, prospects, and challenges, Adv. Mater. **21**, 2632 (2009).

[2] H.-S. P. Wong, H.-Y. Lee, S. Yu, Y.-S. Chen, Y. Wu, P.-S. Chen, B. Lee, F. T. Chen, and M.-J. Tsai, Metal-oxide RRAM, Proc. IEEE **100**, 1951 (2012).

[3] J. J. Yang and R. S. Williams, Memristive devices in computing system: Promises and challenges, ACM J. Emerging Technol. Comput. Syst. **9**, 11 (2013).

[4] D.-H. Kwon, K. M. Kim, J. H. Jang, J. M. Jeon, M. H. Lee, G. H. Kim, X.-S. Li, G.-S. Park, B. Lee, S. Han, M. Kim, and C. S. Hwang, Atomic structure of conducting nanofilaments in $TiO_2$ resistive switching memory, Nat. Nanotechnol. **5**, 148 (2010).

[5] Y. Y. Chen, L. Goux, L. Pantisano, J. Swerts, C. Adelmann, S. Mertens, V. V. Afanas'ev, X. P. Wang, B. Govoreanu, R. Degraeve, S. Kubicek, V. Paraschiv, B. Verbrugge, N. Jossart, L. Altimime, M. Jurczak, J. Kittl, G. Groeseneken, and D. J. Wouters, Scaled X-bar $TiN/HfO_2/TiN$ RRAM cells processed with optimized plasma enhanced atomic layer deposition (PEALD) for TiN electrode, Microelectron. Eng. **112**, 92 (2013).

[6] J. J. Yang, D. B. Strukov, and D. R. Stewart, Memristive devices for computing, Nat. Nanotechnol. **8**, 13 (2013).

[7] A. C. Torrezan, J. P. Strachan, G. Medeiros-Ribeiro, and R. S. Williams, Sub-nanosecond switching of a tantalum oxide memristor, Nanotechnology **22**, 485203 (2011).

[8] J. Borghetti, G. S. Snider, P. J. Kuekes, J. J. Yang, D. R. Stewart, and R. S. Williams, "Memristive" switches enable "stateful" logic operations via material implication, Nature (London) **464**, 873 (2010).

[9] O. Kavehei, E. Linn, L. Nielen, S. Tappertzhofen, S. Skafidas, I. Valov, and R. Waser, Associative capacitive network based on nanoscale complementary resistive switches for memory-intensive computing, Nanoscale **5**, 5119 (2013).

[10] H. Akinaga and H. Shima, Resistive random access memory (ReRAM) based on metal oxides, Proc. IEEE **98**, 2237 (2010).

[11] R. Dittmann, R. Muenstermann, I. Krug, D. Park, T. Menke, J. Mayer, A. Besmehn, F. Kronast, C. M. Schneider, and R. Waser, Scaling potential of local redox processes in memristive $SrTiO_3$ thin-film devices, Proc. IEEE **100**, 1979 (2012).

[12] A. Marchewka, B. Roesgen, K. Skaja, H. Du, C. L. Jia, J. Mayer, V. Rana, R. Waser, and S. Menzel, Nanoionic resistive switching memories: On the physical nature of the dynamic RESET process, Adv. Electron. Mater. **2**, 1500233 (2016).

[13] A. Marchewka, R. Waser, and S. Menzel, in *Proceedings of the International Conference on Simulation of Semiconductor Processes and Devices (SISPAD), Washington DC, 2015* (IEEE, New York, 2015), p. 297.

[14] R. Waser, R. Bruchhaus, and S. Menzel, *Redox-based Resistive Switching Memories* (Wiley-VCH, Weinheim, 2012), p. 683.

[15] S. Menzel, M. Salinga, U. Böttger, and M. Wimmer, Physics of the switching kinetics in resistive memories, Adv. Funct. Mater. **25**, 6306 (2015).

[16] S. Menzel, M. Waters, A. Marchewka, U. Böttger, R. Dittmann, and R. Waser, Origin of the ultra-nonlinear switching kinetics in oxide-based resistive switches, Adv. Funct. Mater. **21**, 4487 (2011).

[17] K. Fleck, U. Böttger, R. Waser, and S. Menzel, Interrelation of sweep and pulse analysis of the SET process in $SrTiO_3$ resistive switching memories, IEEE Electron Device Lett. **35**, 924 (2014).

[18] K. Fleck, U. Böttger, R. Waser, and S. Menzel, SET and RESET kinetics of $SrTiO_3$-based resistive memory devices, Mater. Res. Soc. Symp. Proc. **1790**, 7 (2015).

[19] D. Ielmini, F. Nardi, and S. Balatti, Evidence for voltage-driven SET/RESET processes, IEEE Trans. Electron Devices **59**, 2049 (2012).

[20] T. Diokh, E. Le-Roux, S. Jeannot, C. Cagli, V. Jousseaume, J. F. Nodin, M. Gros-Jean, C. Gaumer, M. Mellier, J. Cluzel, C. Carabasse, P. Candelier, and B. De Salvo, Study of resistive random access memory based on TiN/$TaO_x$/TiN integrated into a 65 nm advanced complementary metal oxide semiconductor technology, Thin Solid Films **533**, 24 (2013).

[21] S. Yu, Y. Wu, and H. Wong, Investigating the switching dynamics and multilevel capability of bipolar metal oxide resistive switching memory, Appl. Phys. Lett. **98**, 103514 (2011).

[22] P. Huang, Y. Wang, H. Li, B. Gao, B. Chen, F. Zhang, L. Zeng, G. Du, J. Kang, and X. Liu, Analysis of the voltage-time dilemma of metal oxide-based RRAM and solution exploration of high speed and low voltage ac switching, IEEE Trans. Nanotechnol. **13**, 1127 (2014).

[23] H. Schroeder, V. V. Zhirnov, R. K. Cavin, and R. Waser, Voltage-time dilemma of pure electronic mechanisms in resistive switching memory cells, J. Appl. Phys. **107**, 054517 (2010).

[24] Y. Nishi, S. Menzel, K. Fleck, U. Boettger, and R. Waser, Origin of the SET kinetics of the resistive switching in tantalum oxide thin films, IEEE Electron Device Lett.. **35**, 259 (2013).

[25] M. D. Pickett, D. B. Strukov, J. L. Borghetti, J. J. Yang, G. S. Snider, D. R. Stewart, and R. S. Williams, Switching dynamics in titanium dioxide memristive devices, J. Appl. Phys. **106**, 074508 (2009).

[26] F. Nardi, S. Larentis, S. Balatti, D. Gilmer, and D. Ielmini, Resistive switching by voltage-driven ion migration in bipolar RRAM Part I: Experimental study, IEEE Trans. Electron Devices **59**, 2461 (2012).

[27] Y. Nishi, K. Fleck, U. Boettger, R. Waser, and S. Menzel, Effect of RESET voltage on distribution of SET switching time of bipolar resistive switching in a tantalum oxide thin film, IEEE Trans. Electron Devices **62**, 1561 (2015).

[28] See Supplemental Material at http://link.aps.org/supplemental/10.1103/PhysRevApplied.6.064015 for measurements on additional materials ($ZrO_x$, and on other different $TaO_x$ and STO stacks). Additional details on the simulations are also provided.

[29] S. Brivio, E. Covi, A. Serb, T. Prodromakis, M. Fanciulli, and S. Spiga, in *Proceedings of the International Conference on Memristive Systems(MEMRISYS) Paphos, Cyprus, 2015* (IEEE, New York, 2015).

[30] Bin Gao, Bing Chen, Yuansha Chen, Lifeng Liu, Xiaoyan Liu, Ruqi Han, and Jinfeng Kang, in *10th IEEE International Conference on Solid-State and Integrated Circuit Technology (ICSICT), Shanghai, China, 2010* (IEEE, New York, 2010).

[31] B. Gao, L. Liu, and J. Kang, Investigation of the synaptic device based on the resistive switching behavior in hafnium oxide, Prog. Nat. Sci. **25**, 47 (2015).

[32] F. Alibart, L. Gao, B. D. Hoskins, and D. B. Strukov, High precision tuning of state for memristive devices by adaptable variation-tolerant algorithm, Nanotechnology **23**, 075201 (2012).

[33] S. Koveshnikov, K. Matthews, K. Min, D. Gilmer, M. Sung, S. Deora, H. Li, S. Gausepohl, P. Kirsch, and R. Jammy, in *Proceedings of the International Electron Devices Meeting (IEDM), San Francisco, 2012* (IEEE, New York, 2012), p. 20.4.1.

[34] M. G. Cao, Y. S. Chen, J. R. Sun, D. S. Shang, L. F. Liu, J. F. Kang, and B. G. Shen, Nonlinear dependence of SET time on pulse voltage caused by thermal accelerated breakdown in the Ti/$HfO_2$/Pt resistive switching devices, Appl. Phys. Lett. **101**, 203502 (2012).

[35] A. Siemon, S. Menzel, A. Marchewka, Y. Nishi, R. Waser, and E. Linn, in *Proceedings of the IEEE International Symposium on Circuits and Systems (ISCAS), Melbourne, 2014* (IEEE, New York, 2014), p. 1420.

[36] V. Longo, M. A. Verheijen, F. Roozeboom, and W. M.M. Kessels, Crystallization study by transmission electron microscopy of $SrTiO_3$ thin films prepared by plasma-assisted ALD, ECS J. Solid State Sci. Technol. **2**, N120 (2013).

[37] N. Aslam, V. Longo, C. Rodenbuecher, F. Roozeboom, W. M.M. Kessels, K. Szot, R. Waser, and S. Hoffmann-Eifert, Impact of composition and crystallization behavior of atomic layer deposited strontium titanate films on the resistive switching of Pt/STO/TiN devices, J. Appl. Phys. **116**, 064503 (2014).

[38] C. Kügeler, J. Zhang, S. Hoffmann-Eifert, S. K. Kim, and R. Waser, Nanostructured resistive memory cells based on 8-nm-thin $TiO_2$ films deposited by atomic layer deposition, J. Vac. Sci. Technol. B **29**, 01AD01 (2011).

[39] A. A. Sharma, M. Noman, M. Abdelmoula, M. Skowronski, and J. A. Bain, Electronic instabilities leading to electro-formation of binary metal oxide-based resistive switches, Adv. Funct. Mater. **24**, 5522 (2014).

[40] M. Noman, A. A. Sharma, Y. M. Lu, M. Skowronski, P. A. Salvador, and J. A. Bain, Transient characterization of the electroforming process in $TiO_2$ based resistive switching devices, Appl. Phys. Lett. **102**, 023507 (2013).

[41] M. Noman, A. A. Sharma, Y. M. Lu, R. Kamaladasa, M. Skowronski, P. A. Salvador, and J. A. Bain, Mechanism of localized electrical conduction at the onset of electroforming in $TiO_2$ based resistive switching devices, Appl. Phys. Lett. **104**, 113510 (2014).

[42] Y. Nishi, S. Schmelzer, U. Böttger, and R. Waser, in *Proceedings of the 43rd European Solid-State Device Research Conference (ESSDERC), Bucharest, 2013* (IEEE, New York, 2013), p. 174.

[43] S. M. Sze and K. K. Ng, *Physics of Semiconductor Devices* (Wiley, New York, 2007).

[44] C. La Torre, K. Fleck, S. Starschich, E. Linn, R. Waser, and S. Menzel, Dependence of the SET switching variability on the initial state in $HfO_x$-based ReRAM, Phys. Status Solidi A **213**, 316 (2016).